Journal of Quantitative Spectroscopy & Radiative Transfer 113 (2012) 2255–2264

Contents lists available at SciVerse ScienceDirect

Journal of Quantitative Spectroscopy & Radiative Transfer

journal homepage: www.elsevier.com/locate/jqsrt

Characterization of spherical core–shell particles by static light scattering. Estimation of the core- and particle-size distributions

Luis A. Clementi [a,b], Jorge R. Vega [a,b,*], Luis M. Gugliotta [a], Arturo Quirantes [c]

[a] INTEC (CONICET and Universidad Nacional del Litoral), Güemes 3450, 3000 Santa Fe, Argentina
[b] FRSF-UTN (Facultad Regional Santa Fe—Universidad Tecnológica Nacional), Lavaisse 610, 3000 Santa Fe, Argentina
[c] Departamento de Física Aplicada (Facultad de Ciencias—Universidad de Granada), Granada 18071, Spain

ARTICLE INFO

Article history:
Received 22 May 2012
Received in revised form
31 July 2012
Accepted 2 August 2012
Available online 10 August 2012

Keywords:
Core–shell particle
Core size distribution
Particle size distribution
Static light scattering
Inverse problem
Tikhonov regularization

ABSTRACT

A numerical method is proposed for the characterization of core–shell spherical particles from static light scattering (SLS) measurements. The method is able to estimate the core size distribution (CSD) and the particle size distribution (PSD), through the following two-step procedure: (i) the estimation of the bivariate core–particle size distribution (C–PSD), by solving a linear ill-conditioned inverse problem through a generalized Tikhonov regularization strategy, and (ii) the calculation of the CSD and the PSD from the estimated C–PSD. First, the method was evaluated on the basis of several simulated examples, with polystyrene–poly(methyl methacrylate) core–shell particles of different CSDs and PSDs. Then, two samples of hematite–Yttrium basic carbonate core–shell particles were successfully characterized. In all analyzed examples, acceptable estimates of the PSD and the average diameter of the CSD were obtained. Based on the single-scattering Mie theory, the proposed method is an effective tool for characterizing core–shell colloidal particles larger than their Rayleigh limits without requiring any *a-priori* assumption on the shapes of the size distributions. Under such conditions, the PSDs can always be adequately estimated, while acceptable CSD estimates are obtained when the core/shell particles exhibit either a high optical contrast, or a moderate optical contrast but with a high 'average core diameter'/'average particle diameter' ratio.

1. Introduction

The particle size distribution (PSD) is a morphological characteristic of primary importance in several particulate systems. For instance, the rheological behavior and chemical stability of paints and inks, the film formation of coatings and its optical properties (such as the gloss), the mechanical properties of adhesives, and the burning rate of fuels and explosives, are all strongly influenced by the PSD [1].

The particle morphology may depend on the specific application of the colloid. Many applications, such as paints, inks, toners and coatings, normally involve spherical homogeneous particles [1]. Nowadays, a growing number of applications require particles with non-homogeneous core–shell morphology. For example, polymeric core–shell particles have been developed as waterborne pressure-sensitive adhesives (PSAs) that can compete with solvent-borne PSAs in high-performance applications [2]. On the other hand, core–shell particles with a core of Ni–Ag bimetallic and a pH-responsive shell of poly(ethylene glycol-*co*-methacrylic acid) have been synthesized for biomedical applications [3]. These particles convert pH changes within cancerous cell to

* Corresponding author at: INTEC (CONICET and Universidad Nacional del Litoral), Güemes 3450, 3000 Santa Fe, Argentina.
Tel.: +54 342 451 1370; fax: +54 342 451 1079.
E-mail addresses: laclementi@santafe-conicet.gov.ar (L.A. Clementi), jvega@santafe-conicet.gov.ar (J.R. Vega), lgug@intec.unl.edu.ar (L.M. Gugliotta), aquiran@ugr.es (A. Quirantes).

0022-4073/$ - see front matter © 2012 Elsevier Ltd. All rights reserved.
http://dx.doi.org/10.1016/j.jqsrt.2012.08.003

fluorescent signals, and therefore they have the ability to light up tumor cells. Additionally, due to their high porosity, these particles might be used for simultaneously delivering anticancer drug molecules into the cancerous cells. Also in biomedical applications, colloids for immunoassays involve spherical particles consisting of a polymeric core (normally polystyrene) coated with a specific antigenic protein, thus exhibiting core–shell morphology [4]. Particles with core of poly(vinylidene fluoride) or poly(butyl acrylate) and shell of polyaniline have recently received great attention due to their ability to form thin films with porous structure for application as gas sensors [5]. In all these applications, the core and shell sizes can directly affect the colloid properties.

Main definitions concerning PSDs in colloids of homogeneous spherical particles were recently reviewed [1]. We shall call $f(D_n)$ the discrete number PSD. The ordinates of $f(D_n)$ represent the number fraction of particles contained in the diameter interval $[D_n, D_n+\Delta D]$ $(n=1,\ldots,N)$, ΔD being a regular partition of the D-axis.

Static light scattering (SLS) is a fast, absolute, non-destructive and highly repetitive technique that has been widely used for characterizing PSDs of colloids [1]. In SLS, the sample is irradiated with a monochromatic beam of wavelength λ_0 and the intensity of the scattered light, I, is measured at several angles, θ_r $(r=1,\ldots,R)$. For homogeneous spherical particles and under single scattering regime [6], the SLS measurement, $I(\theta_r)$, is related to the PSD, $f(D_n)$, through [1]

$$I(\theta_r) = k_I \sum_{n=1}^{N} C_I(\theta_r, D_n, n_{m0}, n_{p0})\ f(D_n) \tag{1a}$$

where k_I is a constant and the coefficient $C_I(\theta_r, D_n, n_{m0}, n_{p0})$ is the light intensity scattered at θ_r by a particle of diameter D_n and refractive index n_{p0} immersed in a non-absorbing medium of refractive index n_{m0}, which is calculated through the Mie scattering theory [6]. SLS is an effective technique for measuring large particles compared to the laser wavelength. In fact, when the laser wavelength outside ($\lambda_{out}=\lambda_0/n_{m0}$) and inside ($\lambda_{in}=\lambda_0/n_{p0}$) the particles is considerably larger than the particles diameter, then the light is scattered according to the Rayleigh regime [6]. Thus, the scattered light intensity is independent of the scattering angle [i.e., $I(\theta_r)$=constant], and therefore no information content on the PSD is included in the SLS measurement.

Eq. (1a) represents a system of R linear algebraic equations with N unknowns (the ordinates of the PSD), which can be written in a matrix form as

$$\mathbf{I} = k_I \mathbf{K} \mathbf{f} \tag{1b}$$

where $\mathbf{I}$ $(R\times 1)$ and $\mathbf{f}$ $(N\times 1)$ contain the discrete heights of $I(\theta_r)$ and $f(D_n)$, respectively, and $\mathbf{K}$ $(R\times N)$ is a matrix with elements given by $K(r,n)=C_I(\theta_r, D_n, n_{m0}, n_{p0})$.

To estimate the PSD from SLS measurements a linear inverse problem must be solved. It consists of inverting Eq. (1a) or (1b) to estimate the PSD, based on the knowledge of the measurement of $I(\theta_r)$ and the Mie coefficients $C_I(\theta_r, D_n, n_{m0}, n_{p0})$. Unfortunately, such inverse problem is ill-conditioned [7]; i.e., small measurement noises can produce large deviations in the estimated PSD.

Several techniques are available for solving linear ill-conditioned inverse problems. Regularization techniques [7] basically involve a least-square minimization of the differences between the measurements and their predictions by Eq. (1), and try to improve the ill-conditioning of the inverse problem by including some *a-priori* knowledge and smoothness conditions on the sought solution. For example, the second-order Tikhonov regularization method [7] can be stated as the following optimization problem:

$$\min_{\hat{\mathbf{f}}} \quad \{\|\mathbf{I} - k_I \mathbf{K}\ \hat{\mathbf{f}}\|^2 + \alpha \|\mathbf{H}\ \hat{\mathbf{f}}\|^2\} \quad \text{subject to } \hat{\mathbf{f}} \geq 0 \tag{2}$$

where the symbol "^" stands for estimated value, α is the regularization parameter that can be calculated through the L-curve method [8], $\mathbf{H}$ $(N\times N)$ is the discrete second derivative operator, and $\|\ \|$ represents the 2-norm of a vector. Clearly, the solution of Eq. (2) will depend on the selected α. While a strong regularization (a large α) produces an excessively smoothened and wide PSD, a weak regularization (a small α) normally originates an oscillatory PSD or the appearance of spurious erroneous modes. The Tikhonov regularization method has been applied to estimate the PSD of homogeneous particles from light scattering measurements [9–12]. To this effect, the optimization problem of Eq. (2) has been solved through several numerical tools, such as artificial neural networks [10], genetic algorithms [11], and the Bayesian methods [12].

Several authors have estimated the sizes of submicrometric homogeneous spherical particles and droplets from SLS measurements [13–15]. For example, Finsy et al. [13] successfully estimated unimodal and multimodal PSDs of polymeric particles through either a maximum entropy method or a constrained regularization technique. Hofer et al. [14] estimated the size distribution of oil droplets in a water emulsion by approximating the PSD by a combination of cubic B-splines. Frontini and Fernandez Berdaguer [15] proposed an iterative procedure for simultaneously estimating the PSD and the refractive index of colloidal particles.

Unlike the case of homogeneous particles, the estimation of sizes in core–shell colloids from SLS measurements has been scarcely studied [16,17]. For instance, Quirantes et al. [16] estimated the PSD of core–shell particles by assuming that the PSD presented a log-normal distribution of mean diameter $\overline{D}$ and a standard deviation σ_D. Then, the parameters $\overline{D}$ and σ_D were adjusted to reproduce the SLS measurements. In that work, one of the following hypothesis was utilized to reduce the number of unknowns in the inverse problem: (i) particles with a unique core diameter $\overline{X}$ (thus reducing the unknowns to three: $\overline{X}$, $\overline{D}$, and σ_D) or (ii) a constant core-to-particle diameter ratio $R=X/D$ (thus reducing the unknowns to three: R, $\overline{D}$, and σ_D). The method acceptably estimated the core and the particle average diameters, but the PSDs resulted broader than those obtained by transmission electron microscopy (TEM). To estimate the PSD of colloidal particles involving a hollow core and a glass shell, Lagasse and Richards [17] assumed a constant ratio X/D, and approximated the PSD by a linear combination of B-splines. The inverse problem was solved through a linear regularization technique that produced PSD estimates with erroneous spurious modes. The method was only applied to the characterization of particles with sizes of several microns. As far as the authors are aware,

there was no attempt to develop a method for simultaneously estimating core and particle sizes without imposing restrictions on the sought size distributions.

In this work, a numerical method is proposed for estimating the core size distribution (CSD) and the PSD of sub-micrometric core–shell spherical particles from SLS measurements. The method is first evaluated through simulated examples that involve CSDs and PSDs of different average sizes and shapes. The incidence of the refractive indexes of the core and shell materials on the estimated size distributions is also investigated. Then, two experimental examples are used for the validation of the method.

2. Core–shell particles: size distributions relationships and SLS model

An arbitrary core–shell spherical particle (with core diameter X_j and particle diameter D_n) is schematically presented in Fig. 1. In general, a colloidal dispersion exhibits a particle population with an ample variety of core and shell sizes. We shall call $F(X_j,D_n)$ the bivariate core–particle size distribution (C–PSD). The ordinates of $F(X_j,D_n)$ represent the number fraction of particles with particle diameters contained in the interval $[D_n,D_n+\Delta D]$ $(n=1,\ldots,N)$ and core diameters contained in $[X_j,X_j+\Delta X]$ $(j=1,\ldots,J)$, where the regular partition of the X-axis (ΔX) can (in general) be different from ΔD. The CSD, $g(X_j)$, and the PSD, $f(D_n)$, can be calculated from $F(X_j,D_n)$, as follows:

$$g(X_j)=\sum_{n=1}^{N} F(X_j,D_n) \tag{3a}$$

$$f(D_n)=\sum_{j=1}^{J} F(X_j,D_n) \tag{3b}$$

Note that $f(D_n)$ corresponds to the outer diameter distribution.

The thickness size distribution (TSD) is defined as the number fraction of particles with shell thicknesses $Z_k=(D_n-X_j)/2$, for $D_n>X_j$, contained in the interval $[Z_k,Z_k+\Delta Z]$ $(k=1,\ldots,K)$, where ΔZ is a regular partition of the Z-axis. Note that particles with different pairs $\{D_n, X_j\}$ can produce the same Z_k. In general, each jth subpopulation (i.e. those particles with a common core diameter X_j) will have a different jth TSD, $h^j(Z_k)$.

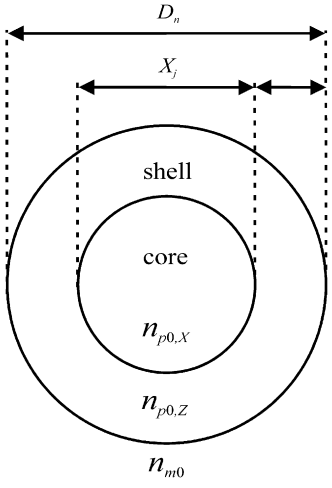

Fig. 1. Schematic representation of a spherical particle with a core–shell morphology.

By assuming that the core sizes and the thickness sizes follow independent distributions, then the C–PSD, the TSD, and the CSD are interrelated through

$$F(X_j,D_n)=g(X_j)\;\; h^j(Z_k)=g(X_j)\;\; h^j[(D_n-X_j)/2] \tag{4}$$

The SLS model of Eq. (1a) can be generalized for particles with core–shell morphologies as follows [16]:

$$I(\theta_r)=k_I\;\sum_{n=1}^{N}\sum_{j=1}^{J} C_I(\theta_r,X_j,D_n,n_{m0},n_{p0,X},n_{p0,Z})F(X_j,D_n) \tag{5}$$

where $C_I(\theta_r, X_j, D_n, n_{m0}, n_{p0,X}, n_{p0,Z})$ is obtained through the Aden and Kerker theory [6], and represents the light intensity scattered at θ_r by a particle with a core of diameter X_j and refractive index $n_{p0,X}$, an outer diameter D_n and a shell of refractive index $n_{p0,Z}$, immersed in a non-absorbing medium of refractive index n_{m0}.

3. The proposed method

In general, Eq. (5) can be used for estimating $F(X_j,D_n)$ from SLS measurements without requiring any *a priori* assumption on its shape. To estimate F, the following generalization of the second-order Tikhonov regularization method [7] is proposed

$$\min_{\hat{F}}\quad \{\|\mathbf{I}-\hat{\mathbf{I}}\|^2+\alpha\textstyle\sum_{n=2}^{N-1}\sum_{j=2}^{J-1}|L[\hat{F}(X_j,D_n)]|^2\};$$
$$\text{subject to}\quad \begin{cases}\hat{F}(X_j,D_n)\geq 0\\ \hat{F}(X_j,D_n)=0 \quad \text{for } X_j>D_n\end{cases} \tag{6}$$

where $\hat{\mathbf{I}}$ $(R\times 1)$ contains the measurements $\hat{I}(\theta_r)$ obtained by injecting the estimated bivariate size distribution $\hat{F}(X_j,D_n)$ into Eq. (5); the restriction $[\hat{F}(X_j,D_n)=0$ for $X_j>D_n]$ is used because the core size X_j cannot be larger than the outer particle diameter D_n; and $L[\hat{F}(X_j,D_n)]$ $(J-2\times N-2)$ is the discrete Laplacian of $\hat{F}(X_j,D_n)$, which is defined as follows:

$$L[\hat{F}(X_j,D_n)]=\hat{F}(X_{j-1},D_n)+\hat{F}(X_{j+1},D_n)+\hat{F}(X_j,D_{n-1})+\hat{F}(X_j,D_{n+1})-4\hat{F}(X_j,D_n) \tag{7}$$

Note that the regularization term of Eq. (6) is only defined for $2\leq n\leq(N-1)$ and $2\leq j\leq(J-1)$, to avoid ambiguities in the calculation of $L[\hat{F}(X_j,D_n)]$.

The regularization parameter, α, can be selected according to the L-curve method [8], as follows: (1) Eq. (6) is solved for a large set of α values, (2) for each α, the corresponding C–PSD estimate, $\hat{F}_\alpha$, is used to evaluate the two terms of Eq. (6): $T_{1,\alpha}=\|\mathbf{I}-\hat{\mathbf{I}}\|^2$ and $T_{2,\alpha}=\sum_{n=2}^{N-1}\sum_{j=2}^{J-1}|L[\hat{F}_\alpha(X_j,D_n)]|^2$, (3) a cubic spline is used to fit $T_{2,\alpha}$ vs. $T_{1,\alpha}$, which produces an L-shaped curve when plotted in a log–log scale, and (4) the final α is chosen as the value corresponding to the maximum curvature point of the L-curve.

The best C–PSD estimate, $\hat{F}(X_j,D_n)$, is assumed to be obtained as the solution of Eq. (6) with the above-selected

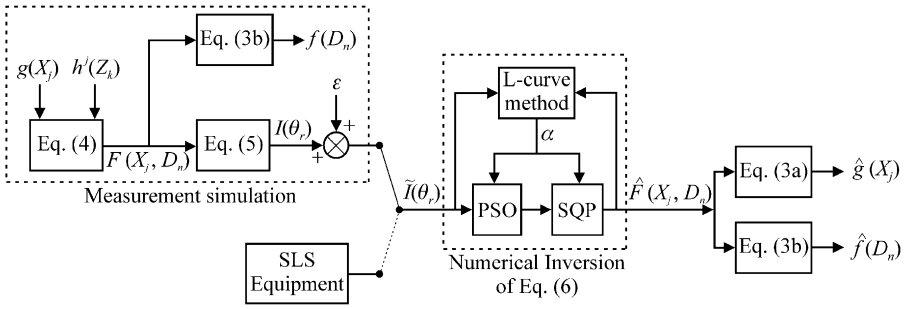

Fig. 2. Schematic data treatment paths for estimating the CSD and the PSD from (simulated or experimental) SLS measurements.

α. Then, the CSD estimate, $\hat{g}(X_j)$, and the PSD estimate, $\hat{f}(D_n)$, are calculated from $\hat{F}(X_j,D_n)$ through Eqs. (3a) and (3b), respectively. Note that the TSDs, $h^j(Z_k)$, and the Eq. (4) are not involved in the estimation procedure; however, they are required in synthetic examples for simulating the C–PSD from the knowledge of both the CSD and the TSD.

In principle, steepest-descent optimization algorithms such as the sequential quadratic programming (SQP) method [18] could be used for solving the linear inverse problem described by Eq. (6). However, the problem involves a huge number of unknowns (the $N \times J$ ordinates of the bivariate size distribution), and the use of a SQP typically requires a high computing time. For this reason, the employment of a stochastic method can be more adequate for obtaining the optimum of Eq. (6) in shorter computing times. In a particle swarm optimization (PSO) algorithm [19], the optimum searching strategy uses a large population of 'particles' (the term 'particle' corresponding to the PSO algorithm will be indicated between apostrophes). Then, in the context of a PSO algorithm, a 'particle' corresponds to an individual; i.e., each 'particle' is a candidate C–PSD to represent the sought solution to the optimization problem.

During the execution of a PSO algorithm, each 'particle' continuously moves through the search space until some relatively stable state is reached [19]. Thus, the lth 'particle' $\mathbf{F}_l$ $(J \times N)$ describes a given trajectory in a $(J \times N)$-dimensional space. The best position reached by the 'particle' $\mathbf{F}_l$ (i.e., the point on its trajectory that minimizes Eq. (6)) is represented by $\mathbf{P}_l$ $(J \times N)$. Similarly, the best position on the whole trajectory set described by the complete 'particle' population is represented by $\mathbf{G}$ $(J \times N)$. The position change rate (or velocity) of any 'particle' $\mathbf{F}_l$ is represented by $\mathbf{V}_l$ $(J \times N)$. Then, the 'particles' are manipulated according to the following model [20]:

$$\mathbf{V}_l(k+1) = w(k)\,\mathbf{V}_l(k) + c_1\,R_1(k)[\mathbf{P}_l(k) - \mathbf{F}_l(k)] + c_2\,R_2(k)[\mathbf{G}(k) - \mathbf{F}_l(k)] \quad (8a)$$

$$\mathbf{F}_l(k+1) = \mathbf{F}_l(k) + \mathbf{V}_l(k+1) \quad (8b)$$

where k represents the iteration number, c_1 and c_2 are two positive constants, $R_1(k)$ and $R_2(k)$ are two random numbers in the range (0,1), and $w(k)$ is the inertial weight [20]. Eq. (8a) is used to calculate the updated 'particle' velocity, $V_l(k+1)$, according to (i) its previous velocity, $V_l(k)$, (ii) its current distance to its best historical position, $[P_l(k) - F_l(k)]$, and (iii) its current distance to the best position found by the whole group, $[G(k) - F_l(k)]$. Then, the 'particle' moves from its old position, $F_l(k)$, to its new position, $F_l(k+1)$, according to Eq. (8b). This process is iteratively repeated until reaching the algorithm convergence, which is assumed to occur when $\boldsymbol{G}$ does not exhibit significant changes. The solution obtained by the PSO is the $\boldsymbol{G}$ value at the last iteration. Since the PSO is a stochastic optimization algorithm, the obtained solution is normally an approximation of the global optimum of Eq. (6). Then, starting from the last $\boldsymbol{G}$, a steepest-descent SQP algorithm is utilized to reach an improved solution.

The proposed method will be validated with both simulated and experimental examples. Fig. 2 summarizes the calculation paths. In simulated examples, $g(X_j)$ and $h^j(Z_k)$ are assumed to be known and Eq. (4) is used to calculate $F(X_j,D_n)$. Then, the simulated PSD, $f(D_n)$, is obtained through Eq. (3b); and the noisy measurement, $\tilde{I}(\theta_r)$, is calculated by adding a random noise ε to the noise-free SLS measurement, $I(\theta_r)$, calculated with Eq. (5). In experimental examples, the SLS equipment directly produces $\tilde{I}(\theta_r)$. From $\tilde{I}(\theta_r)$ the proposed method based on the PSO–SQP algorithm is used to estimate the C–PSD with the regularization parameter α calculated through the L-curve method. Finally, the estimated CSD and PSD are obtained through Eqs. (3a) and (3b), respectively.

4. Validation of the proposed method through simulated examples

Four simulated examples (EX 1, EX 2, EX 3, and EX 4) were implemented for evaluating the performance of the proposed method. All examples aimed at estimating the CSD and the PSD of core–shell particles immersed in water, with a polystyrene (PS) core and a poly(methyl methacrylate) (PMMA) shell. For simplicity, in each example it was assumed that all particles exhibited a common TSD [i.e., $h^j(Z_k) = h(Z_k)$], independently of their core sizes. In all simulated examples, the X_j-axis was regularly spaced each 5 nm in the range 200–600 nm, and the Z_k-axis was regularly spaced each 2.5 nm in the range 5–100 nm.

The CSDs were selected as asymmetrical log-normal distributions given by

$$g_p(X_j) = \frac{\Delta X}{X_j \sigma_{X,p}\sqrt{2\pi}} \exp\left[-\frac{[\ln(X_j/\overline{X}_p)]^2}{2\sigma_{X,p}{}^2}\right] \quad (p = 1,2) \quad (9)$$

with $\overline{X}_1=300$ nm, $\sigma_{X,1}=0.04$, $\overline{X}_2=450$ nm, and $\sigma_{X,2}=0.035$. The simulated TSDs were also represented by asymmetrical log-normal distributions, as follows:

$$h_m(Z_k)=\frac{\Delta Z}{Z_k\sigma_{Z,m}\sqrt{2\pi}}\exp\left[-\frac{[\ln(Z_k/\overline{Z}_m)]^2}{2{\sigma_{Z,m}}^2}\right] \quad (m=1,2) \quad (10)$$

with $\overline{Z}_1=15$ nm, $\sigma_{Z,1}=0.25$, $\overline{Z}_2=30$ nm, and $\sigma_{Z,2}=0.35$. The simulated CSDs and TSDs (Fig. 3) exhibit different widths and size ranges, and were selected to evaluate the ability of the proposed method to deal with different size distributions. Then, the four simulated C–PSDs, F_1, F_2, F_3, and F_4 (Fig. 4a, c, e, and g), were built by combining the CSDs with the TSDs, according to Eq. (4), and define the corresponding simulated examples, as follows: EX 1: $F_1(X_j,D_i)=g_1(X_j)h_1(Z_k)$; EX 2: $F_2(X_j,D_i)=g_1(X_j)h_2(Z_k)$; EX 3: $F_3(X_j,D_i)=g_2(X_j)h_1(Z_k)$; and EX 4: $F_4(X_j,D_i)=g_2(X_j)h_2(Z_k)$.

Simulation of the SLS measurements assumed a vertically-polarized Argon laser of wavelength $\lambda_0=488$ nm. At such λ_0, the refractive indexes were $n_{m0}=1.3368$, for the disperse medium (pure water) [16]; $n_{p0,X}=1.5887$, for the PS core [21]; and $n_{p0,Z}=1.4972$, for the PMMA shell [22]. The measurement angles were selected at regular intervals of 5°, in the range 20–150° (then, $R=27$). These parameters were used to evaluate the C_l kernel of Eq. (5) through the Aden–Kerker theory [6]. The noisy SLS measurements, $\tilde{I}_1$, $\tilde{I}_2$, $\tilde{I}_3$, and $\tilde{I}_4$ (Fig. 4b, d, f, and h), were obtained by contaminating the noise-free measurements, $I(\theta_r)$, with an additive noise, ε, similar to that observed in experiments [11,12], as follows:

$$\tilde{I}(\theta_r)=I(\theta_r)+\varepsilon=I(\theta_r)+0.0025\max[I(\theta_r)]\varepsilon_0\times(r=1,\ldots,R) \quad (11)$$

where ε_0 is a Gaussian random sequence of mean zero and variance one.

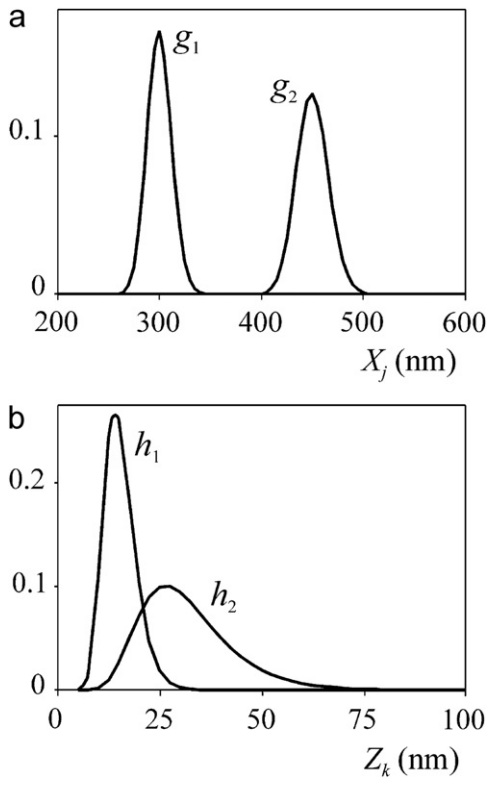

Fig. 3. Simulated (log-normal) CSDs (a) and TSDs (b), used to build the bivariate C–PSD. All distributions were normalized to equal area.

To implement the estimation procedure, wide enough ranges for the X_j and D_n axes must be selected to ensure that they completely contain the simulated CSD and PSD. A common diameter range of 100–800nm (regularly-spaced each 20 nm) was adopted for X_j and D_n.

A PSO with 50 'particles' was utilized to solve the inverse problem. The usual parameters $c_1=c_2=2$ [Eq. (8a)] were directly adopted from literature [20]. The inertia function $w(k)$ was selected as a decreasing linear function from 0.5 (for $k=1$) to 0.1 (for $k=25{,}000$). The PSO algorithm was initialized by assigning to each 'particle' a random bivariate size distribution of components sampled from a uniform distribution. After several runs, it was verified that the PSO reached an acceptable convergence of the objective function in about 25,000 iterations. For this reason, a maximum of 25,000 iterations was adopted as a reliable criterion for stopping the PSO procedure. Then, the approximate solution obtained by the PSO was utilized as the initial guess for obtaining an improved solution of Eq. (6) after application of a SQP algorithm [18].

For each example, the proposed inversion method was applied to estimate the C–PSD, $\hat{F}_i$ $(i=1,\ldots,4)$, from the knowledge of its corresponding noisy measurement, $\tilde{I}_i$ $(i=1,\ldots,4)$. Then, the estimated CSDs, $\hat{g}_p(X_j)$, $(p=1,2)$, and PSDs, $\hat{f}_i(D_n)$, $(i=1,\ldots,4)$, were calculated from Eqs. (3a) and (3b) (see Fig. 2).

The following indexes (J_g and J_f), the number average diameters ($\overline{X}_g$ and $\overline{D}_f$), and the percentage errors ($E_{\overline{X}}$ and $E_{\overline{D}}$), were defined to evaluate the performance of the estimation method:

$$J_g=\left(\frac{\sum_{j=1}^{J}[g(X_j)-\hat{g}(X_j)]^2}{\sum_{j=1}^{J}[g(X_j)]^2}\right)^{0.5} \quad (12a)$$

$$J_f=\left(\frac{\sum_{n=1}^{N}[f(D_n)-\hat{f}(D_n)]^2}{\sum_{n=1}^{N}[f(D_n)]^2}\right)^{0.5} \quad (12b)$$

$$\overline{X}_g=\frac{\sum_{j=1}^{J}X_j\ g(X_j)}{\sum_{j=1}^{J}g(X_j)} \quad (12c)$$

$$\overline{D}_f=\frac{\sum_{n=1}^{N}D_n\ f(D_n)}{\sum_{n=1}^{N}f(D_n)} \quad (12d)$$

$$E_{\overline{X}}=100\frac{|\overline{X}_g-\hat{\overline{X}}_g|}{\overline{X}_g} \quad (12e)$$

$$E_{\overline{D}}=100\frac{|\overline{D}_f-\hat{\overline{D}}_f|}{\overline{D}_f} \quad (12f)$$

Indexes J_g and J_f evaluate the ability of the proposed method to estimate the 'true' CSD and PSD, respectively. Note that in a real measurement, it would be impossible

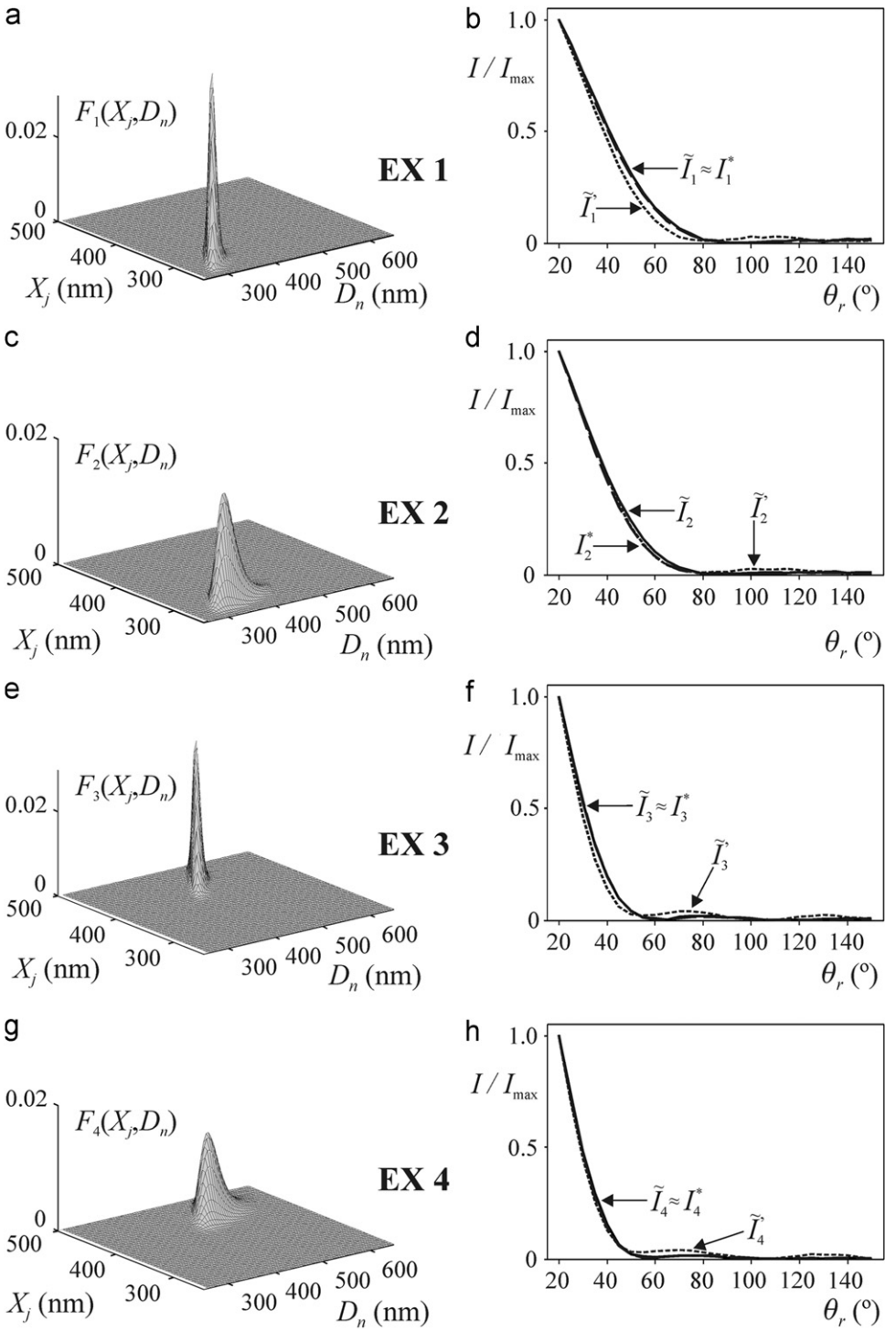

Fig. 4. Four simulated examples: (a, c, e, and g); the bivariate C–PSDs; (b, d, f, and h) the noisy SLS measurements calculated from the C–PSDs and Eq. (5) with particles of moderate ($\tilde{I}$) and high ($\tilde{I}'$) optical contrast. The optical contrast is the difference between refractive indexes of core and shell materials.

to calculate J_g and J_f because the 'true' distributions, $g(X_j)$ and $f(D_n)$, are unknown; however, this criterion was adopted for the simulated examples to investigate the limitations of the estimation method. The errors $E_{\overline{X}}$ and $E_{\overline{D}}$ evaluate the estimation errors of $\overline{X}_g$ and $\overline{D}_f$, respectively.

The main results are presented in Fig. 5 and in Table 1. Fig. 5 shows the simulated CSDs, g_p ($p=1,2$); the 'true' PSDs, f_i ($i=1,\ldots,4$), obtained by inserting the simulated C–PSDs, F_i, into Eq. (3b); and the estimated CSDs, $\hat{g}_p$, and PSDs, $\hat{f}_i$, obtained by inserting the estimated C–PSDs, $\hat{F}_i$,

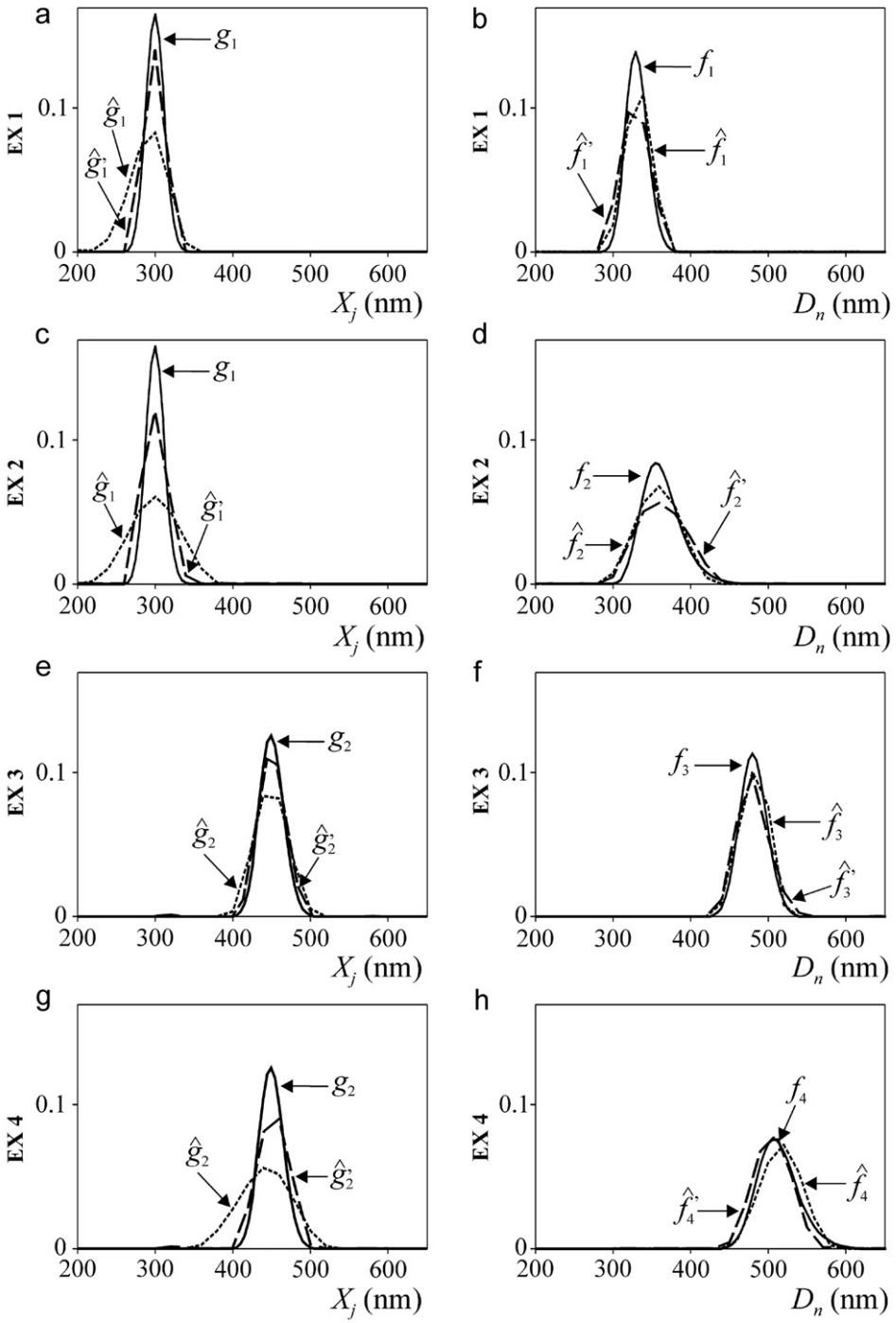

Fig. 5. Estimation results for the four simulated examples with particles of moderate ($\hat{g}_p$ and $\hat{f}_i$) and high ($\hat{g}_p'$ and $\hat{f}_i'$) optical contrasts ($p=1,2$; $i=1,\ldots,4$). (a, c, e, and g); the simulated CSDs and their estimates; (b, d, f, and h) the simulated PSDs and their estimates.

into Eqs. (3a) and (3b). Table 1 shows the resulting performance indexes.

In all the analyzed examples, the estimated PSDs resulted close to the 'true' PSDs (Fig. 5b, d, f, and h). According to Table 1, the following is observed: (i) the average diameters, $\overline{X}_g$ and $\overline{D}_f$, were accurately estimated in the four examples, with a maximum percentage error of 3% in $\overline{X}_g$ and only 1.3% in $\overline{D}_f$; (ii) slightly improved PSD estimates (smaller J_f) were obtained for samples of increasing average diameters; (iii) in samples with a common CSD (EX 1 and EX 2, or EX 3 and EX 4), better CSD estimates (smaller J_g) were obtained when the particles exhibited a small average shell; and (iv) in samples with a common TSD (EX 1 and EX 3, or EX 2

Table 1
Simulated examples. Capability of the numerical method to estimate CSDs and PSDs of core/shell particles with moderate (MC) and high (HC) optical contrasts[a] (numbers between parentheses indicate the true average sizes).

	EX 1		EX 2		EX 3		EX 4	
	MC	HC	MC	HC	MC	HC	MC	HC
J_g (dimensionless)	0.55	0.19	0.65	0.31	0.26	0.07	0.55	0.24
J_f (dimensionless)	0.40	0.43	0.24	0.30	0.22	0.26	0.20	0.17
$\overline{X}_g$ (nm)	291 (300)	299 (300)	300 (300)	300 (300)	449 (450)	451 (450)	440 (450)	451 (450)
$\overline{D}_f$ (nm)	333 (332)	329 (332)	359 (364)	363 (364)	481 (482)	482 (482)	517 (514)	506 (514)
$E_{\overline{X}}$ (%)	3.0	0.3	0	0	0.2	0.2	2.2	0.2
$E_{\overline{D}}$ (%)	0.3	1.2	1.3	0.2	0.2	0	0.6	1.6

[a] The optical contrast is the difference between refractive indexes of the core and the shell materials.

and EX 4), better CSD estimates (smaller J_g) were obtained when the particles exhibited a large average core.

Observations (iii) and (iv) basically indicate that the CSD is better estimated when the ratio 'average core diameter'/'average particle diameter', $\overline{X}_g/\overline{D}_f$, is large. Although rather intuitive, this final observation was reaffirmed through several *ad-hoc* simulations. In fact, based on EX 3, five additional auxiliary examples were generated by successively increasing its average shell thickness. To this effect, five log-normal TSDs, with average shell thickness and standard deviations: {15, 0.50}, {22.5, 0.25}, {22.5, 0.50}, {30, 0.25}, and {30, 0.50}, were combined with the CSD g_2 of EX 3. Then, the method described in Fig. 2 was applied, and the results are summarized in Table 2. The almost constant J_f indicates that the PSD is acceptably estimated independently of the $\overline{X}_g/\overline{D}_f$ ratio. However, the monotonically increasing J_g confirms that the CSD estimate is deteriorated for decreasing $\overline{X}_g/\overline{D}_f$ ratios.

4.1. Influence of the core/shell optical contrast

In all analyzed examples, the core/shell optical contrast (i.e., the difference between refractive indexes of core and shell) is moderate ($n_{p0,X}-n_{p0,Z}=0.0915$). To analyze the effect of the core/shell optical contrast on the quality of the estimated distributions, the following noisy SLS measurements were simulated (see Fig. 4b, d, f, and h): (a) $\tilde{I}_i'$, as obtained from particles with $n_{p0,X}=2.0$ and $n_{p0,Z}=1.4972$ (i.e., with a high optical contrast: $n_{p0,X}-n_{p0,Z}=0.5028$), and (b) $\tilde{I}_i^*$, as obtained from homogeneous PMMA particles with $n_{p0}=1.4972$. While $\tilde{I}_i$ and $\tilde{I}_i^*$ are practically coincident, large differences are observed between $\tilde{I}_i$ and $\tilde{I}_i'$. These results suggest that improved information on the CSD can be retrieved when the particles exhibit a high core/shell optical contrast.

In order to evaluate the effect of the optical contrast on the estimated size distributions, the proposed method was applied to the noisy measurements, $\tilde{I}_i'$. The estimated CSDs, $\hat{g}_p'$, and PSDs, $\hat{f}_i'$, are also shown in Fig. 5, and the corresponding performance indexes are indicated in Table 1. In all cases, the CSD estimates ($\hat{g}_p'$) obtained at high optical contrast (HC) are better than those obtained at moderate optical contrast (MC). Thus, in the more difficult cases of particles with a low $\overline{X}_g/\overline{D}_f$ ratio, acceptable CSD estimates can even be obtained if the particles exhibit a high core/shell optical contrast. On the other hand, the estimated PSDs were close to the 'true' ones,

Table 2
Simulated examples. Influence of the $\overline{X}_g/\overline{D}_f$ ratio on the quality of the estimated CSDs and PSDs.

$\overline{X}_g/\overline{D}_f$	0.94	0.93	0.91	0.90	0.88	0.87
J_g	0.26	0.36	0.39	0.53	0.57	0.59
J_f	0.22	0.18	0.16	0.26	0.24	0.27

and no meaningful influence of an increased optical contrast was detected from the analysis of indexes J_f and $\overline{D}_f$ (Table 1).

Note that all analyzed examples assumed $n_{p0,X}>n_{p0,Z}$. Even though not shown, similar results were obtained when the four examples were investigated with $n_{p0,X}<n_{p0,Z}$.

5. Application to experimental data

The proposed method was also applied to estimate the CSD and the PSD of two samples (S_1 and S_2) that involve core–shell particles dispersed in water, with cores of hematite (Fe_2O_3) and shells of Yttrium carbonate [$Y(OH)CO_3$]. The samples were obtained in two-steps [16]: (i) the synthesis of a colloid of hematite particles (core), and (ii) the addition of two different amounts of Yttrium carbonate (shell) onto the hematite particles. According to the described procedure, both samples exhibit a common CSD and two different TSDs. The CSD and the PSDs were first measured by transmission electron microscopy (TEM); and then acceptably adjusted with a zero-order normal-logarithmic distribution (ZOLD), as follows:

$$g_{TEM}(X_j)=\frac{\Delta X}{\overline{X}\sigma_X e^{\sigma_X^2/2}\sqrt{2\pi}}\exp\left[\frac{-[\ln(X_j/\overline{X})]^2}{2\sigma_X{}^2}\right] \tag{13a}$$

$$f_{s,TEM}(D_n)=\frac{\Delta D}{\overline{D}\sigma_D e^{\sigma_D^2/2}\sqrt{2\pi}}\exp\left[\frac{-[\ln(D_n/\overline{D})]^2}{2\sigma_D^2}\right](s=S_1,S_2) \tag{13b}$$

The adjusted distributions g_{TEM}, $f_{S1,TEM}$, and $f_{S2,TEM}$ are shown in Fig. 6, and their average diameters are indicated in Table 3. The sample S_1 (Fig. 6c) exhibits a narrow PSD, with a mean diameter of 84 nm; while the sample S_2 (Fig. 6f) exhibits a broader PSD, with an average diameter of 147 nm. Since both samples involve a common CSD (Fig. 6b,e), with an average diameter of 56 nm, Fig. 6c,f reveal that S_2 presents a broader TSD than S_1, with a larger average thickness.

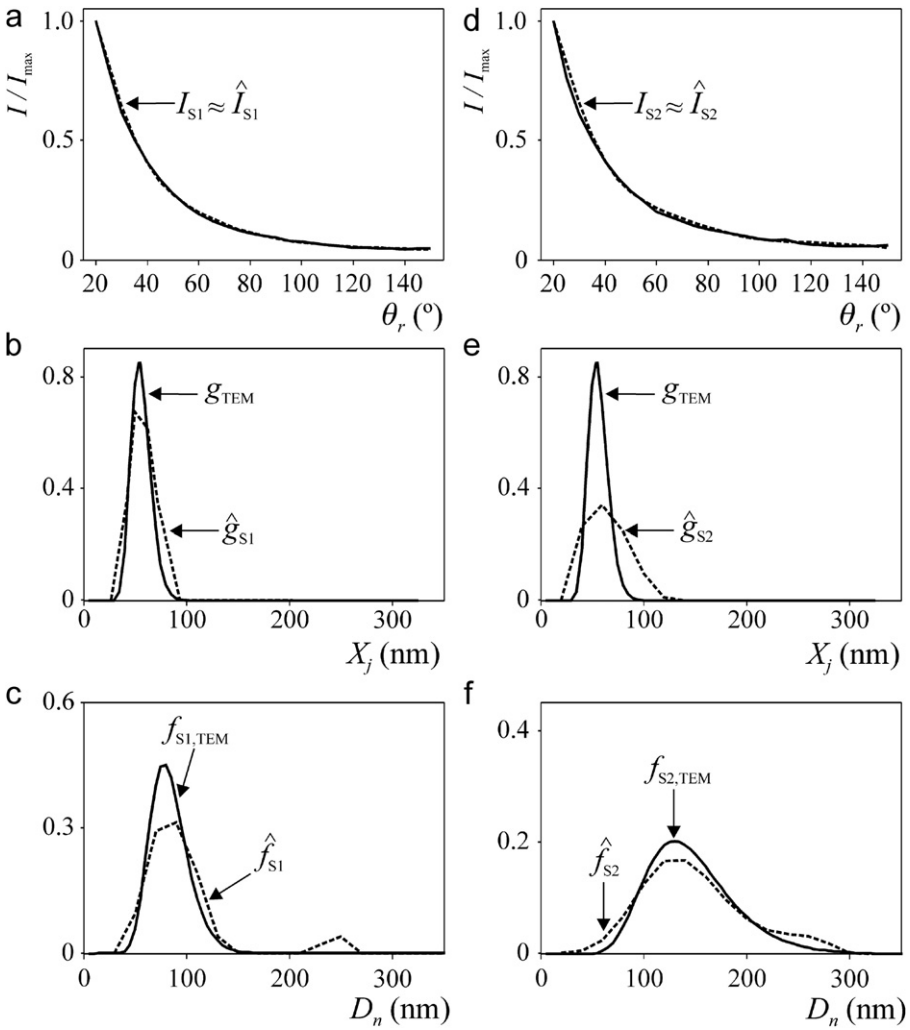

Fig. 6. Experimental samples S_1 and S_2. (a,d) the SLS measurements, I_{S1}, I_{S2}, and their estimates, $\hat{I}_{S1}$, $\hat{I}_{S2}$; (b,e) the 'true' CSD obtained by TEM, g_{TEM}, and its estimates, $\hat{g}_{S1}$, $\hat{g}_{S2}$; (c,f) the PSDs obtained by TEM, $f_{S1,TEM}$ and $f_{S2,TEM}$, and their estimates, $\hat{f}_{S1}$, $\hat{f}_{S2}$.

The SLS measurements were acquired with a Malvern 4700 PCS spectrometer (Malvern Instruments) fitted with a vertically polarized Argon laser (λ_0=488 nm). For this λ_0, the refractive indexes are as follows: n_{m0}=1.3368, for the disperse medium (pure water); $n_{p0,X}$=3.086+0.491 i, for the hematite core; and $n_{p0,Z}$=1.650, for the Yttrium carbonate shell [16]. The nonzero imaginary component in $n_{p0,X}$ indicates that the core material absorbs radiation at λ_0. For the measurement process, the particle concentration was low enough to avoid multiple scattering. The measurement angles were selected at regular intervals of 5°, in the range 20–150° (then, R=27). The obtained SLS measurements, I_{S1} and I_{S2}, are shown in Fig. 6a and d, respectively.

To implement the estimation procedure, a common diameter range of 20–500 nm regularly-spaced each 20 nm was adopted for X_j and D_n. As prescribed in Fig. 2, the following steps were implemented: (1) from I_{S1} and I_{S2}, the C–PSD of samples S_1 and S_2 were obtained through the PSO–SQP algorithm, and (2) the estimated CSDs and PSDs were calculated from Eqs. (3a) and (3b), respectively. The main results are presented in Fig. 6 and in Table 3. The estimated SLS measurements, $\hat{I}_{S1}$ and $\hat{I}_{S2}$, were obtained by replacing the estimated C–PSD into Eq. (5), and are practically superimposed with the measurements I_{S1} and I_{S2} (Fig. 6a,d). In Fig. 6b,e, the estimated CSDs, $\hat{g}_{S1}$ and $\hat{g}_{S2}$, are compared with their TEM distribution, g_{TEM}. In Fig. 6c,f, the estimated PSDs, $\hat{f}_{S1}$ and $\hat{f}_{S2}$, are compared

Table 3
Experimental examples. Capability of the numerical method to estimate the CSDs and PSDs (numbers between parentheses indicate the average sizes obtained by TEM).

	S_1	S_2
J_g (dimensionless)	0.11	0.59
J_f (dimensionless)	0.23	0.15
$\overline{X}_g$ (nm)	56 (56)	64 (56)
$\overline{D}_f$ (nm)	86 (84)	149 (147)
$E_{\overline{X}}$ (%)	0	14.0
$E_{\overline{D}}$ (%)	2.4	1.4

with their TEM distributions, $f_{S1,TEM}$ and $f_{S2,TEM}$. The performance indexes of Table 3 were calculated by assuming that g_{TEM}, $f_{S1,TEM}$ and $f_{S2,TEM}$ are the 'true' distributions.

As in the case of the simulated examples, the best CSD estimate (smallest J_g) was obtained for the sample S_1 that exhibits the highest $\overline{X}_g/\overline{D}_f$ ratio (Fig. 6b,e and Table 3). In contrast, the sample S_2 involved a smaller $\overline{X}_g/\overline{D}_f$ ratio, and the CSD estimate shows more important deviations with respect to g_{TEM}. In both analyzed samples, the CSD average diameters were acceptably estimated (Table 3). Fig. 6c,f indicates that the proposed method produced acceptable PSD estimates. In the case of the sample S_1, an erroneous mode of size 250 nm and number concentration of 6% was estimated as a consequence of the small regularization parameter produced by the L-curve method. This spurious mode could be eliminated by using a stronger regularization (a higher α), but would lead to an artificially-broader PSD estimate.

6. Conclusions

A numerical method was proposed for simultaneously estimating the CSD and the PSD of spherical core–shell particles from SLS measurements. The generalized second-order Tikhonov regularization method together with the PSO–SQP algorithms were effective to solve the ill-conditioned inverse problem. The proposed strategy (Fig. 2) presents the following advantages: (i) no *a-priory* assumption on the shape of the CSD or the PSD is required; (ii) the numerical procedure is of easy computational implementation (routines for the light scattering process, PSO, and SQP are all of public domain); (iii) the estimation procedure can be automated because the L-curve method provides the α regularization parameter without intervention of the user; and (iv) the estimates are practically independent of the selected diameter range. In a standard desktop PC (Intel® Core™ Duo processor), the numerical procedure requires typical computing times of around 5 min to produce the estimated distributions.

For particles beyond the Rayleigh regime, the PSD estimates are always acceptable and the CSD can be adequately estimated when the core/shell particles exhibit either a high optical contrast, or a moderate optical contrast and a high $\overline{X}_g/\overline{D}_f$ ratio. For instance, in the experimental examples, the huge difference between the refractive indexes of core and shell enabled an acceptable CSD estimate in spite of the small $\overline{X}_g/\overline{D}_f$ ratio. For Rayleigh particles, acceptably estimates of the CSD or the PSD are not possible, due to the lack of information on the CSD and the PSD in the SLS measurements.

Acknowledgments

The authors are grateful for the financial support received from CONICET, MinCyT, Universidad Nacional del Litoral, and Universidad Tecnológica Nacional (Argentina).

References

[1] Gugliotta LM, Clementi LA, Vega JR. Particle size distribution. Main definitions and measurement techniques. In: Gugliotta LM, Vega JR, editors. Measurement of particle size distribution of polymer latexes. Kerala: Research Signpost-Transworld Research Network; 2010. p. 1–58.
[2] Foster AB, Lovell PA, Rabjohns MA. Control of adhesive properties through structured particle design of water-borne pressure-sensitive adhesive. Polymer 2009;50:1654–70.
[3] Wu W, Shen J, Gai Z, Hong K, Banerjee P, Zhou S. Multi-functional core–shell hybrid nanogels for pH-dependent magnetic manipulation, fluorescent pH-sensing, and drug delivery. Biomaterials 2011;32:9876–87.
[4] Gonzalez VDG, Garcia VS, Vega JR, Marcipar IS, Meira GR, Gugliotta LM. Inmunodiagnosis of Chagas disease: synthesis of three latex–protein complexes containing different antigens of *Trypanosoma Cruzi*. Colloids Surf B 2010;77:12–7.
[5] Wojkiewicz JL, Bliznyuk VN, Carquigny S, Elkamchi N, Redon N, Lasri T, et al. Nanostructured polyaniline-based composites for ppb range ammonia sensing. Sensors Actuators B 2011;160:1394–403.
[6] Bohren CF, Huffman DH. Absorption and scattering of light by small particles. New York: John Wiley & Sons; 1983.
[7] Aster R, Borchers B, Thurber C. Parameter estimation and inverse problems. USA: Academic Press; 2005.
[8] Hansen PC, O'Leary DP. The use of the L-curve in the regularization of discrete ill-posed problems. SIAM: J Sci Comput 1993;14:1487–503.
[9] Vega JR, Frontini GL, Gugliotta LM, Eliçabe GE. Particle size distribution by combined elastic light scattering and turbidity measurements. A novel method to estimate the required normalization factor. Part Part Syst Charact 2003;20:361–9.
[10] Gugliotta LM, Stegmayer GS, Clementi LA, Gonzales VDG, Minari RJ, Leiza JR, et al. A neural network model for estimating the particle size distribution of dilute latex from multiangle dynamic light scattering measurements. Part Part Syst Charact 2009;26:41–52.
[11] Clementi LA, Vega JR, Gugliotta LM. Particle size distribution of multimodal polymer dispersions by multiangle dynamic light scattering. Solution of the inverse problem on the basis of a genetic algorithm. Part Part Syst Charact 2010;27:146–57.
[12] Clementi LA, Vega JR, Gugliotta LM, Orlande HRBA. Bayesian inversion method for estimating the particle size distribution of latexes from multiangle dynamic light scattering measurements. Chemom Intell Lab Syst 2011;107:165–73.
[13] Finsy R, Deriemaeker L, Gelade E, Joosten J. Inversion of static light scattering measurements for particle size distributions. J Colloids Interface Sci 1992;153:337–54.
[14] Hofer M, Schurz J, Glatter O. Oil–water emulsion: particle size distributions from elastic light scattering data. J Colloids Interface Sci 1989;127:147–55.
[15] Frontini GL, Fernandez Berdaguer EM. Inversion of elastic light scattering measurements to determine refractive index and particle size distribution of polymeric emulsions. J Inverse Probl Eng 2003;11:329–40.
[16] Quirantes A, Plaza R, Delgado A. Static light scattering study of size parameters in core–shell colloidal systems. J Colloids Interface Sci 1997;189:236–41.
[17] Lagasse RR, Richards DW. Determining the size distribution of core–shell spheres and other complex particles by laser diffraction. J Colloids Interface Sci 2003;267:65–73.
[18] Fletcher R. Practical methods of optimization. New York: John Wiley & Sons; 1987.
[19] Rocca P, Benedetti M, Donelli M, Franceschini D, Massa A. Evolutionary optimization as applied to inverse scattering problems. Inverse Probl 2009;25:1–41.
[20] Shi Y, Eberhart R. A modified particle swarm optimizer. In: Proceedings of the IEEE conference on evolutionary computation. Singapore; 1998. p. 69–73.
[21] Inagaki T, Arakawa ET, Hamm RN, Williams MW. Optical properties of polystyrene from the near infrared to the X-ray region and convergence of optical sum rules. Phys Rev B 1977;15:3243–53.
[22] Kasarova SN, Sultanova NG, Ivanov CD, Nikolov ID. Analysis of the dispersion of optical plastic materials. Opt Mater 2007;29:1481–90.